

# Parallel Computation of Power System EMTs through Polyphase-QMF Filter Banks

J. R. Zuluaga, J. L. Naredo, L.J. Castañón, M. Vega, O. Ramos-Leaños

**Abstract**— The analysis of electromagnetic transients in power systems often requires intensive computations. Various methods have been proposed to reduce execution times and computational costs. A new technique is proposed here in which the system model is synthesized in the Laplace domain and is simulated in the time domain through long convolutions. The nodal matrix of the system under analysis is reduced by Kron's method to leave only the nodes related to observations and to changes in explicit form. State vectors derived from the reduced matrix are convolved with auxiliary signals to simulate transient events and the convolutions are performed in parallel by an algorithm based on polyphase QMF filter-banks. The proposed technique is applied in the simulation of a transient on a 17-bus network. The obtained results are compared with those from PSCAD / EMTDC and from the conventional Laplace Transform. Finally, the suitability of this technique for parallel processing is demonstrated by a basic implementation on an FPGA.

**Keywords:** Electromagnetic Transients; Numerical Laplace Transform; parallel processing; real-time; faster than real time; Polyphase QMF filter banks, FPGAs.

## I. INTRODUCTION

The analysis and the simulation of electromagnetic transients (EMT) in power systems often demand lengthy and intensive computations. These tasks usually are carried out through sequential time-domain techniques based mostly in emtp techniques [1], [2]. Certain transient studies could require hundreds of simulations consisting in variations of the same network and the same phenomena; this is the case at statistical studies in insulation coordination [3], [4]. The aim of this paper is to introduce a methodology to reduce computational times and costs in the simulation of EMTs, especially at statistical EMT studies.

Various strategies have been previously developed to reduce the computational times and costs of these tasks [5]. Three of them are identified next. A first strategy consists in dividing a large network into time-decoupled subnetworks that can be computed simultaneously with parallel processors [6]-[8]. A second strategy consists in using network equivalents or simplified models for those subnetworks outside the area of interest of a transient study [9]-[11]. A third strategy is to apply multi-rate techniques for handling slow transient events with larger integration time-steps than for faster events [12]-[15].

One problem with the time-decoupling strategy is that this relies on the presence of long lines or of two-port elements with the proper delays to provide the required time decoupling. It is

then clear that one does not have the control over the size of the decoupled subnetworks and that the computational loads of the parallel processes can be unbalanced. As for the use of network equivalents and simplified models, these are usually represented by rational functions that are prone to passivity-violation problems [11], [16]. Finally, varying time-step and multi-rate techniques are promising; however, their effective application to the analysis and simulation of EMTs in power systems is still at an early stage of development [12]-[15].

To avoid the previous shortcomings, a new technique is proposed here that combines parallel processing, multi-rate techniques and reduction of computational complexity. This technique is based on the premise that transient events can be effectively represented by switch operations. The network under study is first represented by its nodal matrix in the Laplace-domain [2], [17]. This nodal matrix is then reduced by Kron's method [18], leaving in explicit form only the nodes of interest; that is, the ones presenting changes due to transients, as well as those related to observation variables. The reduced nodal form is next modified according to state changes and inverted to produce reduced  $\mathbf{Z}_{red}$  matrices, the columns of each of these matrixes that are involved in a switching event are combined into a single one  $\mathbf{Z}^{(p)}$  characterizing the network response to the switch operation. The elements of  $\mathbf{Z}^{(p)}$  are transformed afterwards to discrete time-domain and switch effects are determined by long convolutions between the  $\mathbf{Z}^{(p)}$  transformed elements and waveforms from auxiliary sources representing the switch operation. Finally, the global response of the network under study to a sequence of transient events is obtained by repeatedly applying superposition [19].

The major computational burden of the technique being proposed here is the execution of the convolutions involved in each transient event. Nevertheless, these convolutions are carried out effectively with a parallel-processing algorithm based on the structure of a bank of polyphase Quadrature-Mirror Filters (QMF) [20]-[23].

The main contribution of this paper is thus the introduction of the previously described methodology that reduces substantially the computational times and costs of EMT simulations often required by statistical studies. The proposed methodology provides full flexibility to apply multi-rate and highly paralleled processes so to attain simulation speeds hundreds of times faster than real-time. An additional feature of the proposed methodology is that, by not requiring the use of rational approximations, it is free from passivity problems. Finally, it should be pointed out that, at its present state of development, this methodology may not be appropriate for long-term simulations (i.e., longer than 1s), as well as for dealing with detailed representations of power electronic devices.

J. R. Zuluaga, J.L. Naredo and L.J. Castañón are with Cinvestav Guadalajara - Mexico (e-mail of corresponding author: jrzuaguad@gmail.com).

M. Vega is with Universidad Autónoma de Guadalajara and O. Ramos-Leaños is with Centre de Recherché de Hydro Québec

Paper submitted to the International Conference on Power Systems Transients (IPST2021) in Belo Horizonte, Brazil June 6-10, 2021.

## II. NETWORK REPRESENTATION

Consider an  $N$ -node network represented in nodal form:

$$\mathbf{I} = \mathbf{Y}_{bus}\mathbf{V} \quad (1)$$

where  $\mathbf{Y}_{bus}$  is the corresponding  $N \times N$  admittance matrix,  $\mathbf{V}$  is the vector of nodal voltages and  $\mathbf{I}$  is the vector of currents being injected into the nodes. It is assumed here that the elements of  $\mathbf{Y}_{bus}$ ,  $\mathbf{V}$  and  $\mathbf{I}$  are in the Laplace domain; *i.e.*, these are functions of the complex variable  $s=c+j\omega$  with its real part “ $c$ ” representing a damping constant and the imaginary part “ $\omega$ ” corresponding to frequency [2], [17].

Electric power networks tend to be very large with a number of nodes in the order of the thousands [3], [4]. The direct solution of (1) can thus be impractical and often requires very long computational times. It is thus proposed to partition  $\mathbf{Y}_{bus}$  of (1) as follows:

$$\begin{bmatrix} \mathbf{I}_1 \\ \mathbf{I}_2 \end{bmatrix} = \begin{bmatrix} \mathbf{Y}_{11} & \mathbf{Y}_{12} \\ \mathbf{Y}_{21} & \mathbf{Y}_{22} \end{bmatrix} \begin{bmatrix} \mathbf{V}_1 \\ \mathbf{V}_2 \end{bmatrix}, \quad (2)$$

where sub-matrix  $\mathbf{Y}_{11}$  involves only the nodes that present changes due to transients (*i.e.*, switching operations), as well as the ones related to observed signals. The order  $N_I \times N_I$  of matrix  $\mathbf{Y}_{11}$  should thus be much smaller than that of  $\mathbf{Y}_{bus}$  [3], [4]. On the other hand,  $\mathbf{Y}_{22}$  includes all the nodes whose voltages are not required explicitly. On applying Kron’s reduction to (2) [18]:

$$\mathbf{I}_1 = \mathbf{Y}_{red}\mathbf{V}_1 + \mathbf{Y}_{12}\mathbf{Y}_{22}^{-1}\mathbf{I}_2 \quad (3)$$

with

$$\mathbf{Y}_{red} = [\mathbf{Y}_{11} - \mathbf{Y}_{12}\mathbf{Y}_{22}^{-1}\mathbf{Y}_{21}]. \quad (4)$$

It follows from (3) that:

$$\mathbf{V}_1 = \mathbf{V}_{SS} + \mathbf{V}_{TR} \quad (5)$$

with

$$\mathbf{V}_{SS} = \mathbf{Z}_{SS}\mathbf{I}_2, \quad (6)$$

$$\mathbf{V}_{TR} = \mathbf{Z}_{red}\mathbf{I}_1 \quad (7)$$

$$\mathbf{Z}_{red} = [\mathbf{Y}_{red}]^{-1} \quad (8)$$

and

$$\mathbf{Z}_{SS} = -\mathbf{Z}_{red}\mathbf{Y}_{12}\mathbf{Y}_{22}^{-1} \quad (9)$$

Note in (5) that the voltage response  $\mathbf{V}_1$  consists of two parts. The first one is the steady state response  $\mathbf{V}_{SS}$  and the second one is a transient disturbance  $\mathbf{V}_{TR}$  due to a switch operation. Usually, the elements of  $\mathbf{I}_2$  are alternating current (AC) pure sinusoids at the nominal frequency  $\omega_0 = 100\pi$  or  $120\pi$  rad/s; the components of  $\mathbf{Z}_{SS}$  are thus constants evaluated at  $\omega_0$ . In the case that the initial steady state is a harmonic state,  $\mathbf{Z}_{SS}$  must be calculated at each harmonic frequency  $k\omega_0$ , with  $k=2, 3, \dots$ , etc, and  $\mathbf{V}_{SS}$  is obtained by superposing the responses of the harmonics.

At the beginning of a study, in the steady state, vector  $\mathbf{I}_1$  in (7) is zero and, consequently,  $\mathbf{V}_{TR}$  is also zero. From this point on, the occurrence of a transient is simulated by switches being represented by current injections at the corresponding nodes. A further consideration for the methodology being presented here is that nonlinear elements are incorporated into the simulations through piecewise-linear representations. This can be done as described in references [19] and [24] and it should be noted that piecewise-linear models involve operating switches.

## III. SWITCH REPRESENTATION

Fig. 1a depicts an open switch at nodes  $k$  and  $l$  of a network and  $v_{kl}(t)$  denotes the voltage difference between its poles. Switch closing can be simulated by connecting a voltage source  $v_{close}(t)$  that neutralizes  $v_{kl}(t)$ , see Fig. 1b:

$$v_{close}(t) = -v_{k,l}(t)u(t - t_{close}) \quad (10)$$

where  $u(t)$  is the unit step function and  $t_{close}$  is the switch closing time [19]. For nodal analysis it is convenient to convert the voltage source at Fig. 1b into its Norton equivalent as in Fig. 1c, with

$$i_{close}(t) = v_{close}(t)/R_{sw} \quad (11)$$

and

$$G_{sw} = 1/R_{sw} \quad (12)$$

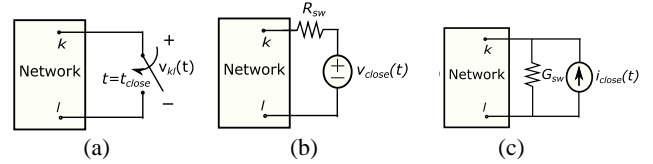


Fig. 1. (a) Closing switch. (b) Closing representation with an auxiliary voltage source (c) Closing switch representation with auxiliary current source.

In the case of an ideal switch, the inclusion of  $G_{sw}$  will introduce an error; this, however, can be minimized by choosing a sufficiently large value for  $G_{sw}$ ; for instance,  $G_{sw} = 10^6 S$ .

Fig. 2a depicts a closed switch between the nodes  $k$  and  $l$  of a network and  $i_{kl}(t)$  represents its current. Switch opening is simulated by injecting a current  $i_{open}(t)$  at nodes  $k$  and  $l$  that neutralizes  $i_{kl}(t)$  (see Fig. 2b):

$$i_{open}(t) = -i_{k,l}(t)u(t - t_{open}) \quad (13)$$

where  $t_{open}$  is the switch opening time.

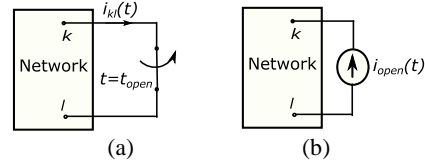


Fig. 2. (a) Closed Switch (b) Simulating switch opening with an auxiliary current source.

The two auxiliary currents,  $i_{close}(t)$  and  $i_{open}(t)$ , are brought into the Laplace domain:

$$I_{open}(s) = \mathcal{L}\{i_{open}(t)\} \quad (14)$$

and

$$I_{close}(s) = \mathcal{L}\{i_{close}(t)\} \quad (15)$$

where  $\mathcal{L}\{\}$  represents the Laplace transform. Lower-case letters represent time domain quantities, while upper-case letters represent their corresponding Laplace domain counterparts. As opposed to the standard method for evaluating EMTs with the Numerical Laplace Transform (NLT) [2], [17], the technique being proposed here does not require the Direct Laplace Transform. Its appearance in (14) and (15) is merely symbolic.

## IV. SIMULATING A SEQUENCE OF TRANSIENT EVENTS

Operation of the above switch model modifies  $\mathbf{Z}_{red}$  (8). Nevertheless, this is a simple process, as one has to apply the

corresponding changes to a maximum of four elements of  $Y_{II}$  in (4), as well as to invert the new low-order  $Y_{red}$  matrix to obtain the  $Z_{red}^{(p)}$  matrix in turn. Therefore, a sequence of  $P$  switch operations can be described as follows:

$$V_1^{(0)} = V_{SS}, \quad (16)$$

$$V_1^{(p)} = Z_{red}^{(p)} I_1^{(p)} + V_1^{(p-1)}, \quad \text{with } p = 1, 2, 3, \dots, P, \quad (17)$$

where  $V_1^{(0)}$  represents the initial voltage response which usually is the steady state and  $Z_{red}^{(p)}$  is the reduced impedance matrix of the system being modified according to switch operations. The calculation of the first term at the right-hand-side of (17) does not require the full multiplication of order  $N_I \times N_I$  matrix  $Z_{red}^{(p)}$  by the order  $N_I$  vector of currents  $I_1^{(p)}$  as this vector has only two non-zero values corresponding to the switch nodes; *i.e.*,  $k$  and  $l$  at Figs. 1c and 2b:

$$V_{TR}^{(p)} = \begin{pmatrix} Z_{1,1}^{(p)} & \dots & Z_{1,k}^{(p)} & \dots & Z_{1,l}^{(p)} & \dots & Z_{1,N_I}^{(p)} \\ Z_{2,1}^{(p)} & \dots & Z_{2,k}^{(p)} & \dots & Z_{2,l}^{(p)} & \dots & Z_{2,N_I}^{(p)} \\ \vdots & & \vdots & & \vdots & & \vdots \\ Z_{N_I,1}^{(p)} & \dots & Z_{N_I,k}^{(p)} & \dots & Z_{N_I,l}^{(p)} & \dots & Z_{N_I,N_I}^{(p)} \end{pmatrix} \begin{pmatrix} \vdots \\ \vdots \\ I_{sw}^{(p)} \\ \vdots \\ -I_{sw}^{(p)} \\ \vdots \end{pmatrix} \begin{matrix} \rightarrow k \\ \\ \\ \rightarrow l \end{matrix} \quad (18)$$

Note that  $I_{SW}^{(p)}$  consists either of current  $I_{close}$  or of  $I_{open}$ , depending on the switch change of state. Since the elements in the vector of currents are zero, except for those at nodes  $k$  and  $l$ , expression (18) can be rewritten as follows:

$$V_{TR}^{(p)} = Z^{(p)} I_{SW}^{(p)} \quad (19)$$

with

$$Z^{(p)} = \begin{bmatrix} Z_1^{(p)} \\ Z_2^{(p)} \\ \vdots \\ Z_{N_I}^{(p)} \end{bmatrix} = \begin{bmatrix} Z_{1,k}^{(p)} - Z_{1,l}^{(p)} \\ Z_{2,k}^{(p)} - Z_{2,l}^{(p)} \\ \vdots \\ Z_{N_I,k}^{(p)} - Z_{N_I,l}^{(p)} \end{bmatrix} \quad (20)$$

Note that  $Z^{(p)}$  is a vector of impedance differences and  $I_{SW}^{(p)}$  is a scalar; therefore, the calculation of the vector of voltages  $V_{TR}^{(p)}$  is no longer the multiplication of a matrix by a vector; it is instead the product of a vector by a scalar and the computational complexity is reduced from  $N_I^2$  to  $N_I$ . With this simplification, base equations (16)-(17) are restated as follows:

$$V_1^{(0)} = V_{SS} \quad (21)$$

$$\text{and } V_1^{(p)} = Z^{(p)} I_{SW}^{(p)} + V_1^{(p-1)}, \quad \text{with } p = 1, 2, \dots, P \quad (22)$$

After applying the inverse Laplace transform to (21) and (22) the base expressions take the following time domain form:

$$v_1^{(0)} = v_{SS} \quad (23)$$

$$\text{and } v_1^{(p)} = \mathfrak{z}^{(p)} * i_{sw}^{(p)} + v_1^{(p-1)}, \quad \text{with } p = 1, 2, \dots, P \quad (24)$$

where “\*” represents convolution;  $\mathfrak{z}^{(p)}$ ,  $v_1^{(p)}$ , and  $i_{sw}^{(p)}$  are the inverse transforms of  $Z^{(p)}$ ,  $V_1^{(p)}$  and  $I_{sw}^{(p)}$ , respectively. Note that (24) represents  $N_I$  scalar equations of the form:

$$v_{1,k}^{(p)} = \mathfrak{z}_k^{(p)} * i_{sw}^{(p)} + v_{1,k}^{(p-1)} \quad (25)$$

As base expressions (23)-(25) are implemented numerically in discrete time, the  $\mathfrak{z}_k^{(p)}$  terms are obtained at a preprocessing stage by applying the Inverse Numerical Laplace Transform (INLT) [16], [19] to the  $Z_k^{(p)}$  terms at (20). The INLT requires to establish the maximum frequency  $\omega_{max}$  (or bandwidth) of the transient phenomenon being considered, as well as the simulation time  $T_{max}$ . Other parameters being needed for the INLT are [2], [17]:

$$N_t = \lceil \omega_{max} \times T_{max} / 2\pi \rceil, \quad (26)$$

$$\Delta t = T_{max} / N_t, \quad (27)$$

$$\Delta \omega = \omega_{max} / N_t \quad (28)$$

$$\text{and } c = \Re\{s\} = [5 \times \ln(10)] / T_{max}. \quad (29)$$

$N_t$  is the number of samples, either in  $Z_k^{(p)}$  or in  $\mathfrak{z}_k^{(p)}$ ,  $\Delta t$  is the time-step,  $\Delta \omega$  is the frequency-step and  $c$  is the damping constant in the complex variable  $s$ . The value of  $c$  in (29) is appropriate for an  $N_t$  between 512 and 2048 samples and the accuracy attained by the INLT is in the order of  $10^{-5}$  [2].

## V. MULTI-RATE AND PARALLEL PROCESSING

Convolutions in (24) and (25) are carried out through the following expression resembling the output of a FIR digital filter [23]:

$$y(n) = \sum_{k=0}^n h(n-k)x(k); \quad n = 1, 2, \dots, N_t - 1, \quad (30)$$

with  $h(n)$  and  $x(k)$  representing  $\mathfrak{z}_k^{(p)}$  and  $i_{sw}^{(p)}$ , respectively (see Fig. 3a).

### A. Polyphase Filters

Consider the following transfer function obtained by applying the Z transform to the filter relation in (30) [23]:

$$H(z) = \sum_{i=0}^{N_t-1} h_i z^{-i}, \quad (31)$$

where  $h_i = h(i)$ . The following regrouping of the filter coefficients is carried out in  $M$  blocks with  $L$  sums each [22]:

$$H(z) = \sum_{k=0}^{M-1} z^{-k} H_k(z^M), \quad (32)$$

$$\text{with } H_k(z^M) = \sum_{l=0}^{L-1} h_{k+lM} z^{-l}, \quad (33)$$

$$\text{and } L = \lceil N_t / M \rceil. \quad (34)$$

The parallel processing structure shown in Figure 3b follows from (32) and (33). This structure can be improved further by simplifying the  $M$  parallel filters  $H_k(z^M)$ . The order of each of these is  $M \times (L-1)$ ; nevertheless, this can be reduced to  $(L-1)$  by the proper introduction of  $M$ -sample decimation and interpolation stages. Hereafter,  $M$  corresponds to the multi-rate, decimation, or parallelization index. Proper introduction of the required decimation and interpolation stages is attained here through a bank of Quadrature-Mirror Filters (QMF) [22], [25].

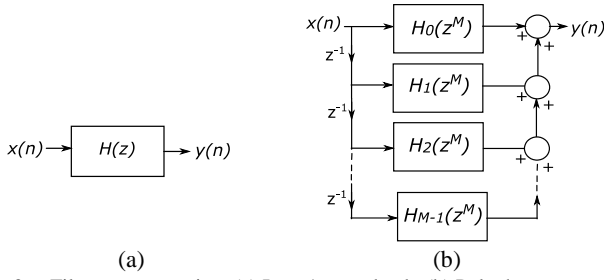


Fig. 3. Filter representation. (a) Input/output block. (b) Polyphase.

### B. QMF Filter Banks.

Fig. 4 shows a QMF filter-bank in cascade-connection with the polyphase filter of Fig. 3b. This is the simplest  $M$ -stage QMF bank [22], [23]. It consists of an arrangement of filters (delays), decimators, and interpolators [20], [25].  $\downarrow M$  represents the decimation operation, *i.e.*, the one in which only the first sample out of each group of  $M$  is kept.  $\uparrow M$  represents the interpolation operation, *i.e.*, the one in which  $M - 1$  zeros are inserted between every two samples of the input signal. The output  $w(n)$  of the QMF filter-bank is simply its input  $x(n)$  delayed  $M - 1$  time-steps [21], [22], [25]:

$$w(n) = x(n - M + 1) \quad (35)$$

or, in the  $Z$  transform domain:

$$Y(z) = X(z)z^{-M+1} \quad (36)$$

The decimation and interpolation blocks of the QMF filter bank are time-varying processes which in general cannot be commuted with other filters; nevertheless, since at each polyphase filter the  $z$  variable appears as a power of  $M$  one can appeal to Noble's identity to perform the desired commutations [22]-[25]. This results in the structure of Fig. 5 that enables the parallel computation of the convolutions in (24) and (25), along with the polyphase filter simplification. Note however that the output of the system depicted by Fig. 5 has been affected by a delay of  $M-1$  time-steps.

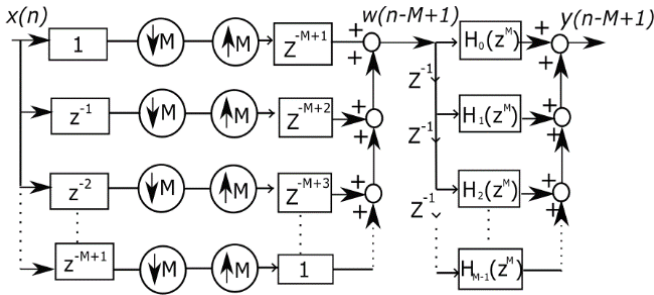


Fig. 4. Cascade connection of a QMF Filter-Bank and a polyphase filter.

### C. Computational Complexity of the Polyphase-QMF Filter Bank.

According to (30), the calculation of  $y(n)$  requires  $n$  multiplications and  $n-1$  additions; thus, the following number of sums is needed to obtain all the outputs, from  $n = 0$  to  $N_t$ :

$$(N_t^2 - N_t) / 2; \quad (37)$$

this along with the following number of multiplications:

$$(N_t^2 + N_t) / 2; \quad (38)$$

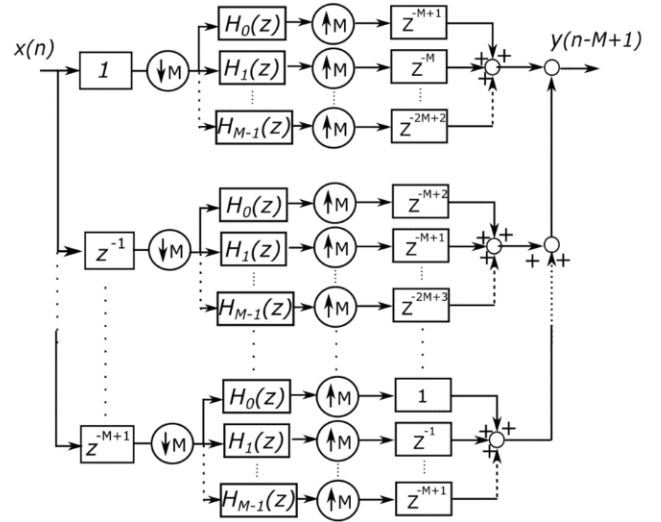


Fig. 5. Polyphase-QMF filter-bank.

As the convolution is implemented using the structure of Figure 5, this requires the execution of  $M^2$  convolution threads in parallel; however, each of these threads is for  $L=N_t/M$  samples and, therefore, the total number of sums being performed is:

$$M^2[(L)^2 - L]/2 = [N_t^2 - MN_t]/2, \quad (39)$$

and the number of multiplications is:

$$M^2[(L)^2 + L]/2 = [N_t^2 + MN_t]/2 \quad (40)$$

Under the premise that at (37) to (40) the quadratic term prevails over the first degree term, it is concluded that both implementations, the direct one of (38) and the parallel one of Fig. 5, perform the same number of operations; However, the computation time of the direct implementation will be proportional to  $N_t^2$  while that of the parallel one is proportional to  $L^2 = (N_t/M)^2$ . This means that with the structure of the polyphase-QMF filter-bank, the processing speed increases  $M^2$  times. Recall that  $M$  is the decimation or parallelization factor being used. Table I presents a comparison of the number of operations between both processes, the direct one and the parallel one being proposed.

TABLE I  
DIRECT VS. PARALLEL CONVOLUTIONS

	Direct Structure	Polyphase filter Banks
<b>Additions</b>	$(N_t^2 - N_t)/2$	$[N_t^2 - MN_t]/2 + M$
<b>Multiplications</b>	$(N_t^2 + N_t)/2$	$[N_t^2 + MN_t]/2$
<b>Acceleration Factor</b>	1	$M^2$

Although the  $M^2$  speed-increase factor is attained at the cost of having  $M^2$  processes in parallel, this is each time less of a limitation due to the continuous and sustained progress of parallel processing hardware. Currently, for example, an NVIDIA Tesla K20 GPU-card can run up to 26,624 processes in parallel; this is, in the order of  $2^{14}$  processes [26].

One important issue regarding the proposed parallel process is that the data output is affected by an  $(M-1)$ -sample delay. Nevertheless, this delay becomes irrelevant in practice when compared to the  $M^2$  speed-increase factor being obtained. Thus, this delay can be amply compensated.

## VI. APPLICATION CASE

### A. Test Network

Fig. 6 presents the one-line diagram of a network composed of 12 overhead transmission lines, 3 underground cables and four generators with their respective transformers for a total of 17 three-phase nodes. The underground cables and the overhead transmission lines are modeled in the discrete Laplace domain using a two-port nodal representation and their parameters are calculated according to the data in Figs. 7 and 8 [27]. Table II provides the parameters of the transformers and generators, whereas Table III presents the values of the loads in the system. Finally, Table IV specifies the lengths of each line (TL) and each cable (CL).

Cables are composed of a core and a sheath (see Fig. 7) and the sheaths are considered solidly grounded at both ends. The aerial lines have two ground wires (see Fig. 8) which are considered solidly grounded at transmission towers.

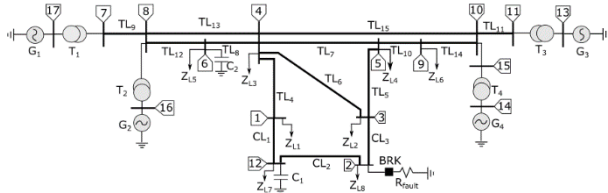


Fig. 6. One-line diagram of test network.

TABLE II  
GENERATOR AND TRANSFORMER DATA.

Generator	Value [PU]
$G_1$	$1.03 \angle 20.2^\circ; Z_{G1}: 1.2\Omega, 38.98mH$
$G_2$	$1.01 \angle 10.5^\circ; Z_{G1}: 1.1\Omega, 45.52mH$
$G_3$	$1.03 \angle -6.8^\circ; Z_{G1}: 0.9\Omega, 38.98mH$
$G_4$	$1.01 \angle -17^\circ; Z_{G1}: 0.8\Omega, 35.23mH$
Transformer	Value [PU]
$T_1$	$Z_{T1}: 1.5\Omega, 23.4mH$
$T_2$	$Z_{T2}: 0.8\Omega, 29.5mH$
$T_3$	$Z_{T3}: 1.6\Omega, 23.4mH$
$T_4$	$Z_{T4}: 0.6\Omega, 35.23mH$

TABLE III  
LOAD DATA.

Load	$Z_{L1}$	$Z_{L2}$	$Z_{L3}$	$Z_{L4}$	$Z_{L5}$
R [ $\Omega$ ]	1200	2150	250	350	350
L [mH]	500	380	25	60	25
Load	$Z_{L6}$	$Z_{L7}$	$Z_{L8}$	$C_1$	$C_2$
R [ $\Omega$ ]	420	200	650	-	-
L [mH]	30	130	250	-	-
C [ $\mu F$ ]	-	-	-	5	20

TABLE IV  
LINE AND CABLE LENGTHS.

Line	$CL_1$	$CL_2$	$CL_3$	$TL_4$	$TL_5$	$TL_6$	$TL_7$	$TL_8$
Length [Km]	10	15	20	150	120	400	220	35
Line	$TL_9$	$TL_{10}$	$TL_{11}$	$TL_{12}$	$TL_{13}$	$TL_{14}$	$TL_{15}$	
Length [Km]	10	35	15	65	133	42	375	

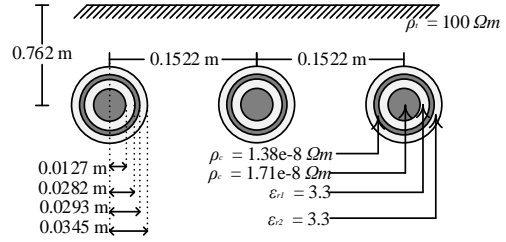


Fig. 7. Transversal layout and electrical data for transmission cables.

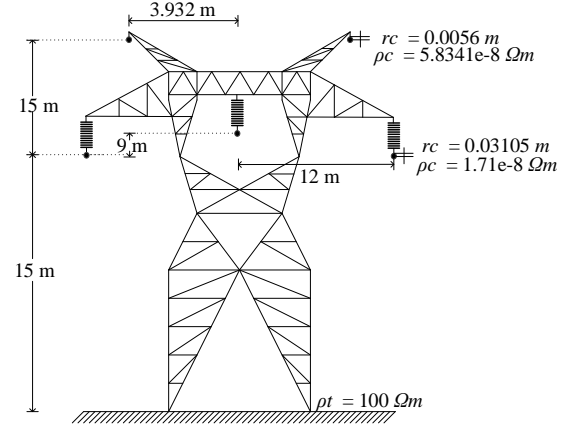


Fig. 8. Transversal layout and electrical data of overhead lines. Conductor heights are medium (or average) heights.

### B. Simulation using a conventional CPU

Fig. 6 network is considered initially at its AC-60 Hz steady state ( $t=0$ ); after a time  $t=22.4ms$  the BRK switch at node 2 closes simulating a three-phase-to-ground fault with a fault resistance  $R_{fault}=5\Omega$ ; subsequently, the fault clears at time  $t=44.3ms$ . Figs 9 and 10 show the voltage waveforms for nodes 2 and 12, respectively. These results are obtained with a desktop computer (CPU) based on an Intel i7 processor, 2.8 GHz and 8 GB RAM. Three different methods have been used to conduct the simulation: 1) the proposed method with polyphase-QMF filter-banks and decimation factors  $M = 1, 8, 32, 64$  and  $128$ ; 2) the conventional NLT [2], [17] without Kron reduction and sequential processing; 3) the PSCAD/EMTDC® program. Maximum relative differences between the proposed method and PSCAD/EMTDC for the results of Fig.9 are 0.0056 for phase a, 0.0033 for phase b and 0.012 for phase c. As for the results of Fig. 10, these differences are 0.0056 for phase a, 0.002 for phase b and 0.0073 for phase c. All these differences are within an acceptable range and are possibly due to differences in the calculation of line and cable parameters between the methods being compared. In sum, the results of Figs. 9 and 10 show that the three methods agree well, thus validating the one proposed here.

The proposed method and the NLT method, have been implemented in MATLAB with simulation time  $T_{max} = 60 ms$ , number of samples  $N_t=4096$  and time-step  $\Delta t=14.65\mu s$ . For the PSCAD® simulation the same  $\Delta t$  is used and the number of samples is increased to  $N_t=4250$ . The execution time for the PSCAD/EMTDC® simulation was 2.55 s. Timing tests were further made for the proposed method with MATLAB and the Parallel Computing Toolbox for the decimation indexes  $M = 1, 2$  and  $4$ . Their respective execution times were 226 ms, 82.2 ms and 31.7 ms.

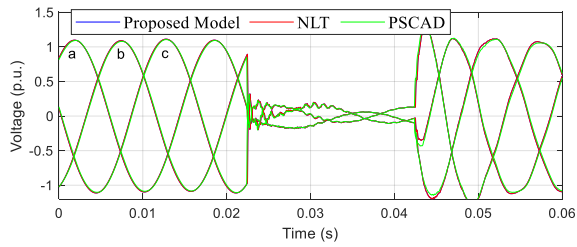


Fig. 9. Voltage responses at node 2 in PU.

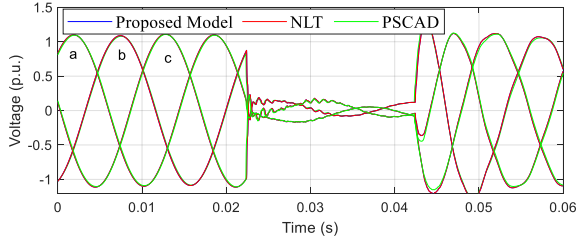


Fig. 10. Voltage responses at node 12 in PU.

Figure 11 shows the waveforms obtained with the proposed method for phase a at node 12 and with decimation factors  $M = 8, 32, 64$  and  $128$ . These waveforms are plotted without compensating the delay given by (35) and it is verified that the use of decimation factors does not affect the precision of the proposed method.

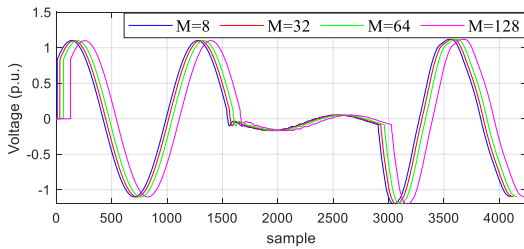


Fig. 11. Voltage response at phase a of node 2 using decimation factors  $M = 8, 32, 64$  and  $128$ .

### C. Parallel Hardware Implementation

The suitability of the proposed method for parallel processors is demonstrated through an elementary implementation of Fig. 6 network model in a basic field programmable gate array (FPGA), a Virtex-6 XC6VLX240T-1FFG1156 with a clock frequency of  $60$  MHz. Due to the limitations of the available FPGA, the implementation was done with fixed point arithmetic and 24 bit word-length.

The network in Fig. 6 is considered initially in the zero-state and a simultaneous energization occurs at time  $t=0$ . This simulation is carried out in the FPGA with a decimation factor  $M=2$ . It is also performed with PSCAD/EMTDC® as well as with the conventional NLT without Kron reduction. The simulation time is  $T_{max} = 40$  ms and the time-step is  $\Delta t = 78.125 \mu s$ ; this results in  $N_t = 512$  samples and a bandwidth of  $12.8$  kHz. Fig. 12 provides the three-phase voltage waveforms at node 1. A good agreement is seen between the three methods. The maximum relative differences between the FPGA results and PSCAD/EMTDC are 0.012 for phase a, 0.0027 for phase b and 0.0076 for phase c. These differences are possibly due to the use of fixed-point Arithmetic and 24 bit word-length in the FPGA simulation; this is in addition to the differences in the calculation of the line and cable parameters

between both methods. FPGA simulation time was of  $21.7 \mu s$  which amounts to 1843 times the real-time speed. This confirms the ability of the proposed technique to perform simulations both, in real time and in faster than real-time.

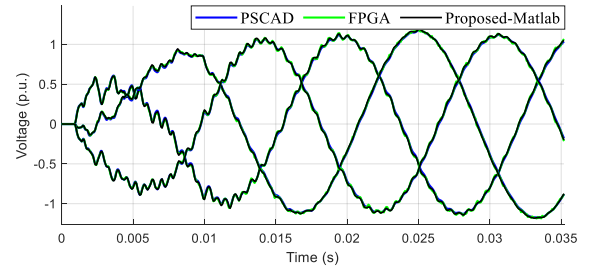


Fig. 12. FPGA simulation and comparison with NLT and PSCAD/EMTDC®.

## VII. CONCLUSIONS

In this paper, a new parallel-processing technique has been proposed to decrease computational times and costs involved in the analysis and simulation of power system EMTs. Its major field of applications is at statistical studies to execute hundreds of EMT simulations that involve variations of the same network and the same phenomena. In this technique, the model for the network under study is synthesized offline in the Laplace domain, avoiding all instabilities associated to time-domain methods, and it is executed in the time domain through long convolutions. Unlike other methods proposed elsewhere, the parallelization technique used here is independent of the topology of the network under study and does not require time-decoupling elements, such as long lines. This feature enables the computational-load balancing of the parallel processes involved in a simulation.

Computational-complexity reduction has been achieved through Kron's method. This avoids resorting to rational equivalents and reduced-order models that are prone to passivity violations. Multiresolution analysis has been introduced in the proposed technique through algorithms based on polyphase-QMF filter banks. These algorithms have provided speed-increase factors proportional to  $M^2$ , being  $M$  the parallelization (or decimation) index. Although this factor is attained at the cost of running  $M^2$  parallel processes (threads), this is each time less of a limitation due to the continuous and sustained progress of parallel processing hardware.

The technique being proposed here has been applied in the simulation of a transient on a 17-bus network including full frequency-dependent lines and cables. The simulation results have been compared satisfactorily well with those from PSCAD/EMTDC®, as well as from the conventional NLT technique without Kron reduction. The affinity of the proposed technique with parallel processors has been further demonstrated by an elementary implementation of it in a basic FPGA. This implementation has attained simulation speeds that are 1843 times faster than real time.

Finally, at its present state of development, the proposed method may not be appropriate for both, long term simulations (i.e., longer than, say, 1 s) and EMT simulations requiring the detailed modeling of power electronic-based devices. These two topics could be subjects for future research.

## VIII. REFERENCES

- [1] Hermann W. Dommel, *EMTP-Theory Book*, Bonneville Power Administration, Portland, OR, USA, 1996.
- [2] Martinez-Velasco, Juan A., *Transient Analysis of Power Systems: Solution Techniques, Tools and Applications*, John Wiley & Sons, 2014.
- [3] H. Khalilnezhad, M. Popov, L. van der Sluis, J. A. Bos and A. Ametani, "Statistical Analysis of Energization Overvoltages in EHV Hybrid OHL-Cable Systems," *IEEE Trans. Power Delivery*, vol. 33, no. 6, pp. 2765-2775, Dec. 2018.
- [4] Mestas, Patricia, and Maria Cristina Tavares, "Relevant parameters in a statistical analysis-Application to transmission-line energization." *IEEE Trans. Power Delivery*, vol. 29, no. 6, pp. 2605-2613, 2014.
- [5] M. Armstrong, J. R. Marti, L. R. Linares and P. Kundur, "Multilevel MATE for efficient simultaneous solution of control systems and nonlinearities in the OVNI simulator," *IEEE Trans. Power Systems*, vol. 21, no. 3, pp. 1250-1259, Aug. 2006
- [6] Z. Zhou and V. Dinavahi, "Parallel Massive-Thread Electromagnetic Transient Simulation on GPU," in *IEEE Transactions on Power Delivery*, vol. 29, no. 3, pp. 1045-1053, June 2014.
- [7] T. Duan, Z. Shen and V. Dinavahi, "Multi-Rate Mixed-Solver for Real-Time Nonlinear Electromagnetic Transient Emulation of AC/DC Networks on FPGA-MPSoC Architecture," in *IEEE Power and Energy Technology Systems Journal*, vol. 6, no. 4, pp. 183-194, Dec. 2019
- [8] M. Matar and R. Iravani, "The Reconfigurable-Hardware Real-Time and Faster-Than-Real-Time Simulator for the Analysis of Electromagnetic Transients in Power Systems," in *IEEE Transactions on Power Delivery*, vol. 28, no. 2, pp. 619-627, April 2013.
- [9] M. Kizilcay, "Low-order network equivalents for electromagnetic transients studies", *European Trans. on Electrical Power*, 3(2), pp.. 123-129, 1993.
- [10] M. Matar and R. Iravani, "A Modified Multiport Two-Layer Network Equivalent for the Analysis of Electromagnetic Transients," in *IEEE Transactions on Power Delivery*, vol. 25, no. 1, pp. 434-441, Jan. 2010.
- [11] D. Shu, X. Xie, Z. Yan and V. Dinavahi, "A Two-Layer Network Equivalent With Local Passivity Compensation With Applications to Hybrid Simulations of MMC-Based AC-DC Grids," in *IEEE Transactions on Power Systems*, vol. 34, no. 6, pp. 4514-4524, Nov. 2019
- [12] A. Semlyen and F. de Leon, "Computation of electromagnetic transients using dual or multiple time steps," *IEEE Trans. on Power Systems*, vol. 8, no. 3, pp. 1274-1281, Aug. 1993.
- [13] H. Zini and G. Ratta, "Multirate modeling scheme for electromagnetic transients calculation," *IEEE Trans. on Power Delivery*, vol. 19, no. 1, pp. 240-247, Jan. 2004.
- [14] H. Ye, K. Strunz, "Multi-scale and frequency-dependent modeling of electric power transmission lines", *IEEE Trans. on Power Delivery*, vol.33, no 1, pp. 32-41, 2018.
- [15] T. Cheng, T. Duan and V. Dinavahi, "Parallel-in-Time Object-Oriented Electromagnetic Transient Simulation of Power Systems," *IEEE Open Access Journal of Power and Energy*, vol. 7, pp. 296-306, 2020.
- [16] S. Grivet-Talocia, B. Gustavsen, *Passive macromodeling: Theory and applications*. John Wiley & Sons, 2015.
- [17] P. Moreno and A. Ramirez, "Implementation of the Numerical Laplace Transform: A Review", *IEEE Trans. on Power Delivery*, vol. 23, no. 4, pp. 2599-2609, Oct. 2008.
- [18] Dörfler, Florian, and Francesco Bullo. "Kron Reduction of Graphs With Applications to Electrical Networks." *IEEE Trans. on Circuits and Systems*, vol. 60, no. 1, pp. 150-163, 2013.
- [19] Pablo Moreno, Pablo Gómez, José L. Naredo, J. L. Guardado, "Frequency domain transient analysis of electrical networks including non-linear conditions", *International Journal of Electrical Power and Energy Systems*, Vol. 27, Issue 2, pp. 139-146, Feb. 2005.
- [20] R. E. Crochiere and L. R. Rabiner, *Multirate Digital Signal Processing*, Prentice-Hall Inc., Upper Saddle River, New Jersey 1983
- [21] N. J. Fliege, *Multirate digital signal processing*, vol. 994, New York: John Wiley, 1994.
- [22] M. Vetterli., "A theory of multirate filter banks," *IEEE Trans. on Acoustics, Speech and Signal Processing*, vol.35-3, pp.356-372, Mar 1987.
- [23] John G. Proakis, Dimitris G. Manolakis, *Digital Signal Processing*, 4<sup>th</sup> Ed., Prentice Hall, 2007.
- [24] C. M. Luna, P. Moreno and J. R. Loo-Yau, "Transformer model with saturation effects for frequency-domain transients simulation," in *IET Generation, Transmission & Distribution*, vol. 11, no. 1, pp. 49-56, 2017
- [25] J. R. Zuluaga and J. L. Naredo, "Poly-phase filter-bank realization for the simulation of electric-network transients," 11th International Conference on Electrical Engineering, Computing Science and Automatic Control (CCE), Campeche, 2014.
- [26] GPU Tesla K20, Datasheet NVIDIA. <https://www.orbitalstore.mx/nvidia/tesla-k20.html>.
- [27] J.A. Martinez-Velasco, *Power System Transients: Parameter Determination*, CRC Press, Boca Raton FL, 2009.